Published paper

Amyotrophic lateral sclerosis-associated mutant VAPBP56S perturbs calcium homeostasis to disrupt axonal transport of mitochondria

Gábor M. Mórotz[1,†], Kurt J. De Vos[1,*,†,‡], Alessio Vagnoni[1], Steven Ackerley[1], Christopher E. Shaw[2] and Christopher C.J. Miller[1,2,*]

[1]Department of Neuroscience and [2]Department of Clinical Neurosciences, Institute of Psychiatry, Kings College London, London, UK

A proline-to-serine substitution at position 56 in the gene encoding vesicle-associated membrane protein-associated protein B (VAPB; VAPBP56S) causes some dominantly inherited familial forms of motor neuron disease, including amyotrophic lateral sclerosis (ALS) type-8. Here, we show that expression of ALS mutant VAPBP56S but not wild-type VAPB in neurons selectively disrupts anterograde axonal transport of mitochondria. VAPBP56S-induced disruption of mitochondrial transport involved reductions in the frequency, velocity and persistence of anterograde mitochondrial movement. Anterograde axonal transport of mitochondria is mediated by the microtubule-based molecular motor kinesin-1. Attachment of kinesin-1 to mitochondria involves the outer mitochondrial membrane protein mitochondrial Rho GTPase-1 (Miro1) which acts as a sensor for cytosolic calcium levels ($[Ca^{2+}]c$); elevated $[Ca^{2+}]c$ disrupts mitochondrial transport via an effect on Miro1. To gain insight into the mechanisms underlying the VAPBP56S effect on mitochondrial transport, we monitored $[Ca^{2+}]c$ levels in VAPBP56S-expressing neurons. Expression of VAPBP56S but not VAPB increased resting $[Ca^{2+}]c$ and this was associated with a reduction in the amounts of tubulin but not kinesin-1 that were associated with Miro1. Moreover, expression of a Ca^{2+} insensitive mutant of Miro1 rescued defective mitochondrial axonal transport and restored the amounts of tubulin associated with the Miro1/kinesin-1 complex to normal in VAPBP56S-expressing cells. Our results suggest that ALS mutant VAPBP56S perturbs anterograde mitochondrial axonal transport by disrupting Ca^{2+} homeostasis and effecting the Miro1/kinesin-1 interaction with tubulin.

INTRODUCTION

Axonal transport of mitochondria is essential for neuronal health and survival since mitochondria need to distribute to axonal regions where their functions in ATP synthesis and Ca^{2+} buffering are needed the most. Compared with most cells, neurons have high metabolic and Ca^{2+}-buffering requirements. Thus, mitochondria are transported bi-directionally through axons and this movement is responsive to physiological stimuli (1).

The microtubule-based motor kinesin-1 mediates most anterograde transport of mitochondria (2–7). One route whereby mitochondria attach to kinesin-1 involves Miro1 and trafficking kinesin protein-1 (TRAK1); Miro1 is an outer mitochondrial membrane protein and TRAK1 is an adaptor protein that binds to both Miro1 and kinesin-1 (2,7–15). Increased $[Ca^{2+}]c$ halts mitochondrial transport and this involves Miro1 which contains two EF hands that bind Ca^{2+} and enable it to act as a Ca^{2+} sensor (8,11,16–19).

*To whom correspondence should be addressed at: Department of Neuroscience P037, Institute of Psychiatry, Kings College London, De Crespigny Park, Denmark Hill, London SE5 8AF, UK. Tel: +44 2078480393; Fax: +44 2077080017; Email: chris.miller@kcl.ac.uk (C.C.J.M.); Email: kurt.de_vos@kcl.ac.uk (K.J.D.V.)
†These authors contributed equally to this work.
‡Present address: Department of Neuroscience, Sheffield Institute for Translational Neuroscience, The University of Sheffield, 385A Glossop Road, Sheffield S10 2HQ UK.
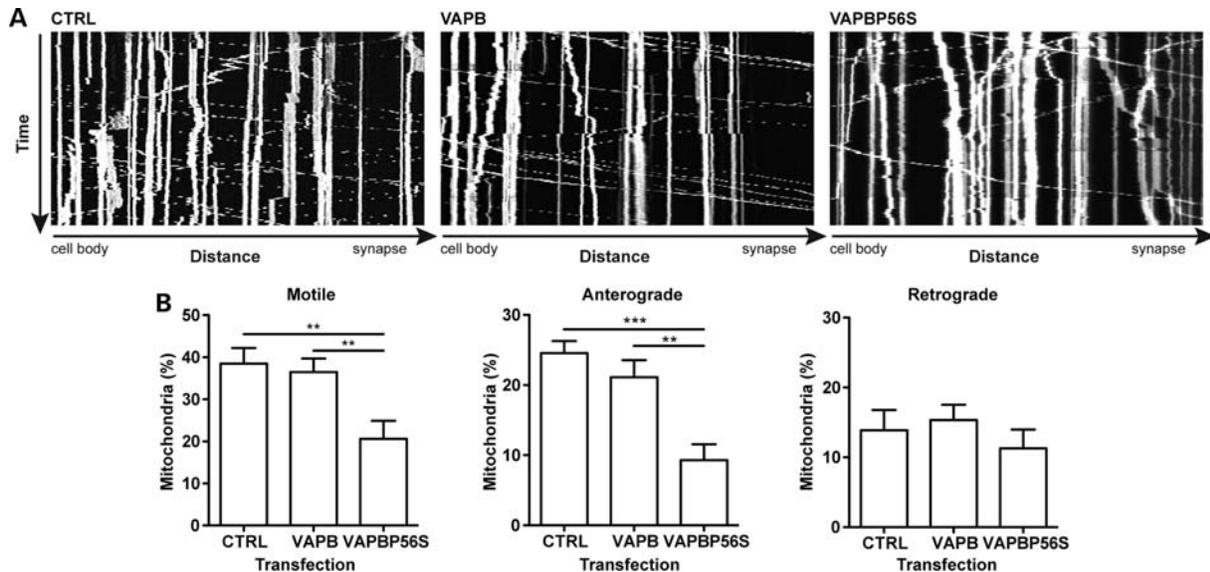
Figure 1. VAPBP56S disrupts anterograde axonal transport of mitochondria. Mitochondrial transport was recorded in neurons co-transfected with DsRed-Mito and either EGFP (CTRL), EGFP-VAPB (VAPB) or EGFP-VAPBP56S (VAPBP56S) as indicated. (**A**) Representative kymographs show axonal transport of mitochondria in EGFP, VAPB or VAPBP56S transfected neurons. (**B**) The percentages of motile, anterograde and retrograde moving mitochondria are shown. Expression of VAPB had no effect on mitochondrial transport. In contrast, VAPBP56S reduced mitochondrial transport and this was due to a selective inhibition of anterograde but not retrograde transport. Statistical significance was determined by one-way ANOVA followed by Tukey's *post hoc* test. $n = 11–14$ cells; error bars are SEM. $**P < 0.01$; $***P < 0.001$.

Defective axonal transport of mitochondria is seen in a number of human motor neuron diseases (20–25). Amyotrophic lateral sclerosis (ALS) is the most common adult onset form of motor neuron disease and some forms of ALS are familial. A mutation in the gene encoding vesicle-associated membrane protein-associated protein B (VAPB) causes some dominantly inherited forms of motor neuron disease, including ALS type-8 (26). VAPB is an integral endoplasmic reticulum (ER) protein and the ALS8 mutation involves a proline-to-serine substitution at position-56 (VAPBP56S). VAPBP56S induces the formation of abnormal ER-derived inclusions (26–31). The function of VAPB is not properly understood; there is evidence that it has roles in ER stress, ER to Golgi transport, bouton formation at the neuromuscular junction, Ca^{2+} homeostasis and signaling via ephrin receptors (29,32–40). Likewise, the precise mechanism by which VAPBP56S induces disease is not known, although several studies implicate a role for ER stress in this process (41). Here, we show that VAPBP56S reduces anterograde axonal transport of mitochondria and that this involves disruption to cellular Ca^{2+} homeostasis.

RESULTS

VAPBP56S selectively disrupts anterograde axonal transport of mitochondria

To investigate any effect of VAPB and VAPBP56S on axonal transport of mitochondria, we quantified mitochondrial transport through axons of living transfected rat cortical neurons by time-lapse microscopy essentially as described in our previous studies (20). Neurons were co-transfected with DsRed-Mito (to visualize mitochondria) and either control vector (vector expressing enhanced green fluorescent protein; EGFP), EGFP-VAPB or EGFP-VAPBP56S. In line with our previous work (42,43), we chose cells expressing low levels of transfected proteins (as judged by brightness of EGFP signal) for analyses to avoid any possible artifacts produced by high-level expression. Several groups have now successfully utilized EGFP tagging to study VAPB/VAPBP56S metabolism (26,36,38,44,45).

We analyzed the overall transport of mitochondria from kymographs by calculating the distance between the position of individual mitochondria at the start and end of time-lapse recordings and dividing by the time elapsed. This yielded an average transport velocity for each mitochondrion that includes anterograde and retrograde movements and stationary periods. Mitochondria were classified as motile when their velocity exceeded 0.1 μm/s or as stationary when their velocity was ≤0.1 μm/s. Quantification of the overall transport of mitochondria revealed that in control axons ∼38% of mitochondria were motile with ∼24 and 14% moving in anterograde and retrograde directions, respectively (Fig. 1). These findings are in agreement with previous studies (20). Expression of VAPB had no significant effect on mitochondrial transport. However, expression of VAPBP56S induced a significant decrease in total mitochondrial motility and this was due to a selective reduction in the number of anterograde moving mitochondria (Fig. 1).

VAPBP56S decreases the frequency, velocity and persistence of anterograde mitochondrial movement

To analyze the features underlying the anterograde axonal transport defect in VAPBP56S-expressing neurons, we determined the positions of all mitochondria at each time point in

Table 1. VAPBP56S decreases the frequency of anterograde mitochondrial movement events

Motile Transfection	Frequency (events/ mitochondria/min)	SD	*P*-value	Anterograde Frequency (events/ mitochondria/min)	SD	*P*-value	Retrograde Frequency (events/ mitochondria/min)	SD	*P*-value
Ctrl	4.089	6.28		2.793	5.42		0.784	1.84	
VAPB	4.733	6.78	ns	3.234	6.11	ns	1.196	3.00	ns
VAPBP56S	2.031	4.40	<0.001	0.726	2.64	<0.001	0.856	2.48	ns

Frequencies of movement were quantified in DsRed-Mito plus either EGFP (control; Ctrl), EGFP-VAPB (VAPB) or EGFP-VAPBP56S (VAPBP56S) co-transfected neurons. VAPBP56S induced a significant decrease in the frequency of anterograde movements without affecting retrograde movement. Statistical significance was determined by the one-way ANOVA (Kruskal–Wallis) test followed by Dunn's multiple comparison test; ns, not significant.

Table 2. VAPBP56S increases the duration of stationary periods between mitochondrial movements

Transfection	Time (s)	SD	*n* (events)	*P*-value
Ctrl	45.95	98.07	2106	
VAPB	58.77	129.90	1805	ns
VAPBP56S	79.71	151.20	753	<0.001

The duration of stationary periods between movements was quantified for mitochondria in DsRed-Mito plus either EGFP (control; Ctrl), EGFP-VAPB (VAPB) or EGFP-VAPBP56S (VAPBP56S) co-transfected neurons. The duration of stationary periods between movements was significantly reduced by VAPBP56S. Statistical significance was determined by the one-way ANOVA (Kruskal–Wallis) test followed by Dunn's multiple comparison test; *n* = 11–14 cells. ns, not significant.

the time-lapse recordings and, from this information, calculated the frequency of anterograde and retrograde movement events, the duration of stationary periods between movements, the velocities of movement and the persistence of unidirectional continuous movements. The transport frequency is an indicator of the regulation of mitochondrial transport (activation versus inactivation) and the persistence is an indicator of motor processivity. We applied a velocity threshold of 0.3 μm/s between successive time points to define movement events. This threshold was set to only include microtubule-based movements, since the reported velocity of actin-based transport of mitochondria is well below 0.3 μm/s (46).

The overall (anterograde and retrograde combined), anterograde and retrograde frequencies of movement events were not significantly different between control EGFP and VAPB transfected neurons (Table 1). In contrast, expression of VAPBP56S reduced the overall mitochondrial transport activity by ~50%, and this was caused by a selective inhibition to anterograde but not retrograde transport activity (Table 1). This reduction in the frequency of anterograde movement events in VAPBP56S-expressing cells was accompanied by a significant increase in the amount of time that mitochondria spent pausing (Table 2). Similar analyses revealed that compared with control EGFP and VAPB transfected neurons, VAPBP56S significantly reduced the velocity and persistence of anterograde but not retrograde mitochondrial movement (Tables 3 and 4). Thus, the disruption to anterograde mitochondrial transport induced by VAPBP56S is a consequence of reductions in the frequency, velocity and persistence of anterograde mitochondrial movements.

VAPBP56S decreases the amount of tubulin but not kinesin-1 associated with Miro1

The microtubule molecular motor kinesin-1 drives most anterograde axonal transport of mitochondria, and attachment of kinesin-1 to mitochondria involves the outer mitochondrial protein Miro1 and the adaptor protein TRAK1 (2,7–15). Two known routes whereby anterograde transport of mitochondria by kinesin-1 can be disrupted involve release of kinesin-1 from Miro1 or release of mitochondria containing the Miro1/TRAK1/kinesin-1 complex from microtubules (8,19). We therefore monitored the effect of VAPB and VAPBP56S expression on the amounts of kinesin-1 and tubulin that were associated with Miro1 in immunoprecipitation experiments. To do so, HEK293 cells were co-transfected with myc-tagged Miro1 (myc-Miro) and hemagglutinin-tagged TRAK1 (HA-TRAK1), and either control vector, VAPB or VAPBP56S, and myc-Miro1 immunoprecipitated using the myc-tag. The amounts of co-immunoprecipitating endogenous kinesin-1 and α-tubulin were then detected by immunoblotting. Others have used similar immunoprecipitation assays to investigate how alterations to signaling pathways influence binding of kinesin-1 motor complexes to tubulin and axonal transport of mitochondria (47). Likewise, since the Miro1/TRAK/kinesin-1 complex is highly conserved in different organisms and cell types, others have used HEK293 cells to dissect the mechanisms that control the association of Miro1 with kinesin-1 and tubulin (8). Expression of VAPB or VAPBP56S did not alter the amounts of kinesin-1 that were associated with myc-Miro1 in these experiments (Fig. 2). Rather, expression of VAPBP56S but not VAPB reduced the amounts of tubulin associated with myc-Miro1 (Fig. 2). This reduction was observed when the amounts of tubulin were normalized to the amounts of both immunoprecipitated Miro1 and co-immunoprecipitated kinesin-1. The reduction in tubulin association with Miro1 was not due to an effect of VAPBP56S on TRAK1 because the levels of TRAK1 found in Miro1 immunoprecipitates were unaffected by VAPBP56S (Fig. 2). Thus, expression of VAPBP56S does not alter the amounts of kinesin-1 or TRAK1 that are associated with Miro1, but rather reduces the amount of tubulin that is associated with the Miro1/TRAK1/kinesin-1 complex.

VAPBP56S increases resting cytosolic Ca²⁺ levels

Elevation of [Ca²⁺]c disrupts anterograde axonal transport of mitochondria (8,11,16–19). Ca²⁺-mediated disruption to

Table 3. VAPBP56S decreases the velocity of anterograde mitochondrial movement

Transfection	Anterograde Velocity (μm/s)	SD	n (events)	P-value	Retrograde Velocity (μm/s)	SD	n (events)	P-value
Ctrl	0.78	0.37	5249		0.75	0.40	2592	
VAPB	0.80	0.39	4938	ns	0.77	0.41	2765	ns
VAPBP56S	0.68	0.37	1157	<0.001	0.78	0.42	1255	ns

Velocities were quantified in DsRed-Mito plus either EGFP (control; Ctrl), EGFP-VAPB (VAPB) or EGFP-VAPBP56S (VAPBP56S) co-transfected neurons. VAPBP56S induced a significant decrease in the velocity of anterograde movements without affecting retrograde velocity. Statistical significance was determined by the one-way ANOVA (Kruskal–Wallis) test followed by Dunn's multiple comparison test; $n = 11-14$ cells. ns, not significant.

Table 4. VAPBP56S decreases the persistence of anterograde mitochondrial movement

Transfection	Anterograde Time (s)	SD	n (events)	P-value	Retrograde Time (s)	SD	n (events)	P-value
Ctrl	8.20	13.46	1928		5.50	5.88	1422	
VAPB	9.18	15.08	1624	ns	5.75	6.06	1456	ns
VAPBP56S	5.96	10.04	563	<0.01	5.74	6.32	664	ns

The persistence of continuous unidirectional movement was quantified in DsRed-Mito plus either EGFP (control; Ctrl), EGFP-VAPB (VAPB) or EGFP-VAPBP56S (VAPBP56S) co-transfected neurons. VAPBP56S induced a significant decrease in the persistence of anterograde movements, but did not affect the persistence of retrograde transport. Statistical significance was determined by the one-way ANOVA (Kruskal–Wallis) test followed by Dunn's multiple comparison test; $n = 11-14$ cells. ns, not significant.

mitochondrial transport can involve release of mitochondria with attached Miro1/TRAK1/kinesin-1 from microtubules (8). Since VAPBP56S-induced disruption to mitochondrial transport likewise involved a reduction in the amount of tubulin associated with the Miro1/TRAK1/kinesin-1 complex (Fig. 2), we monitored the effect of VAPB and VAPBP56S expression on resting $[Ca^{2+}]$c levels in transfected neurons by Fura2 ratio imaging. To ensure that only viable cells were analyzed, we induced a transient Ca^{2+} influx by depolarization with 50 mM KCl; only cells that showed a transient increase in $[Ca^{2+}]$c were included in the analyses of resting $[Ca^{2+}]$c. Expression of VAPB did not change resting $[Ca^{2+}]$c compared with EGFP-transfected control neurons. However, expression of VAPBP56S significantly elevated resting $[Ca^{2+}]$c (Fig. 3). Thus, VAPBP56S-induced disruption to anterograde axonal mitochondrial transport is associated with an increase in resting $[Ca^{2+}]$c.

Expression of a Ca^{2+}-insensitive mutant of Miro1 rescues the effects of VAPBP56S on the association of tubulin with Miro1 and on mitochondrial motility

These results are consistent with a model in which VAPBP56S elevates $[Ca^{2+}]$c to cause release of mitochondria with associated Miro1/TRAK1/kinesin-1 from microtubules to disrupt axonal transport. Elevation of $[Ca^{2+}]$c has been shown to induce release of mitochondria with associated Miro1/TRAK1/kinesin-1 from tubulin (8). Since elevated $[Ca^{2+}]$c disrupts kinesin-1-based transport of mitochondria via an effect on the Miro1 EF hands (8,11,19), we enquired whether expression of a mutant Miro1 in which the EF hands were disrupted could rescue the effect of VAPBP56S on mitochondria

transport. This mutant Miro1 (Miro1[E208K/E328K]) has essential glutamates in the EF hands altered to lysines to inhibit binding of Ca^{2+} (7). Like wild-type Miro1, Miro1[E208K/E328K] supports axonal transport of mitochondria but rescues the effect of elevated $[Ca^{2+}]$c on mitochondrial transport in a number of experimental paradigms (8,11,19).

We monitored the effect of Miro1[E208K/E328K] on the binding of TRAK1, kinesin-1 and tubulin in control, VAPB- and VAPBP56S-expressing cells in immunoprecipitation assays. HEK293 cells were co-transfected with myc-Miro1[E208K/E328K] and HA-TRAK1, and either control vector, VAPB or VAPBP56S and the amounts of endogenous kinesin-1 and tubulin associated with immunoprecipitated myc-Miro1[E208K/E328K] determined by immunoblotting. The amounts of co-immunoprecipitated HA-TRAK1, kinesin-1 and tubulin were not significantly different in any of these cells (Fig. 4). Thus, while VAPBP56S reduces the amount of tubulin associated with wild-type Miro1 (Fig. 2), this effect lost in cells expressing Miro1[E208K/E328K].

To determine whether Miro1[E208K/E328K] could also rescue the effect of VAPBP56S on defective anterograde mitochondrial axonal transport, we co-transfected neurons with DsRed-Mito and either VAPB and control vector, VAPBP56S and control vector, VAPBP56S and Miro1, or VAPBP56S and Miro1[E208K/E328K] and quantified axonal transport of mitochondria. Compared with VAPB-expressing neurons, VAPBP56S again reduced anterograde mitochondrial transport, and this was unaffected by expression of Miro1. However, co-expression of Miro1[E208K/E328K] significantly increased anterograde mitochondrial transport in the VAPBP56S-expressing cells (Fig. 5). Thus, Miro1[E208K/E328K] rescues defective axonal transport of mitochondria in VAPBP56S-expressing neurons.
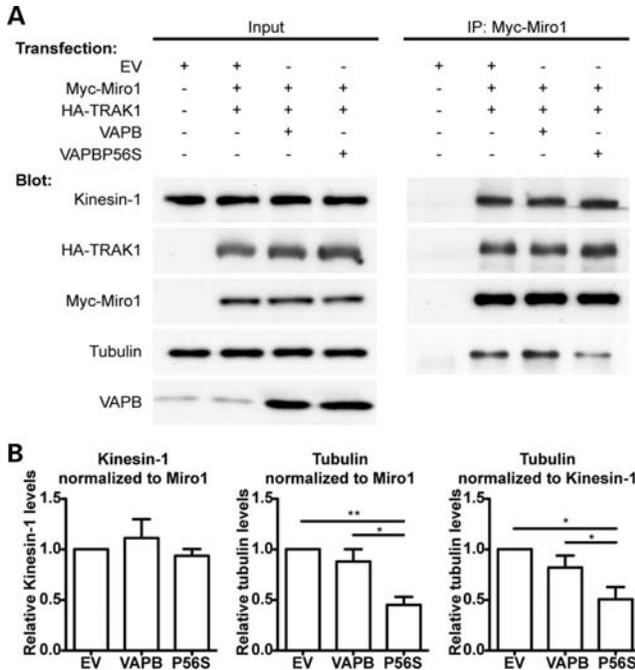
Figure 2. VAPBP56S reduces the amount of endogenous tubulin but not endogenous kinesin-1 associated with Miro1. (**A**) HEK293 cells were co-transfected with either empty vector (EV), empty vector + Myc-Miro1 + HA-TRAK1, VAPB + Myc-Miro1 + HA-TRAK1 or VAPBP56S + Myc-Miro1 + HA-TRAK1 as indicated. Miro1 was immunoprecipitated using the myc-tag and the amounts of co-immunoprecipitating kinesin-1 and α-tubulin detected by immunoblotting. Samples of the input lysates (Input) and immunoprecipitates (IP:Myc-Miro1) are shown. (**B**) Bar graphs show the relative levels of kinesin-1 and α-tubulin in the immunoprecipitates. Kinesin-1 signals were normalized to immunoprecipitated myc-Miro1 signal; α-tubulin signals were normalized to both immunoprecipitated myc-Miro1 and immunoprecipitated kinesin-1 signals as indicated. Values were converted so that empty vector + Myc-Miro1 + HA-TRAK1 transfection was assigned a reference value of 1.0. The results shown are from four independent transfections. Statistical significance was determined by one-way ANOVA followed by Tukey's *post hoc* test. $n = 4$; error bars are SEM. $*P < 0.05$; $**P < 0.01$.

Figure 3. Expression of VAPBP56S increases resting $[Ca^{2+}]c$ levels in neurons. Neurons were transfected with either control EGFP vector, EGFP-VAPB (VAPB) or EGFP-VAPBP56S (P56S) and $[Ca^{2+}]c$ determined by Fura2 ratio imaging. Resting $[Ca^{2+}]c$ was calculated for each individual neuron as the average resting $[Ca^{2+}]c$ between 60 and 180 s of measurement (indicated with box in (**A**)). Values for individual cells were then collated to generate the bar graph in (**B**). To ensure that resting $[Ca^{2+}]c$ was obtained from viable neurons, we induced a transient influx of Ca^{2+} by a 2 min application of 50 mM KCl to depolarize the neurons. Only cells that showed a transient increase in $[Ca^{2+}]c$ after depolarization were included in the analysis of resting $[Ca^{2+}]c$. Statistical significance was determined by one-way ANOVA (Kruskal–Wallis) followed by Dunn's multiple comparison test. $n = 10$ (CTRL), 14 (VAPB) and 20 (VAPBP56S) cells; error bars are SEM. $*P < 0.05$.

DISCUSSION

The molecular mechanisms that underlie motor neuron demise in ALS are not properly understood but damage to axonal transport, mitochondria and Ca^{2+} homeostasis are all acknowledged to be early pathological features of the disease (48,49). Here, we show that VAPBP56S which causes some dominantly inherited familial forms of motor neuron disease including ALS type-8 damages axonal transport of mitochondria. Disruption to mitochondrial transport was directional involving perturbation to anterograde but not retrograde movement. Mutations in the gene encoding Cu/Zn superoxide dismutase-1 (SOD1) also cause familial ALS, and mutant SOD1 likewise perturbs anterograde but not retrograde axonal transport of mitochondria (20). Thus, two different genetic insults associated with ALS both damage axonal transport of mitochondria in similar fashions.

This selective effect on anterograde transport suggests that VAPBP56S may target kinesin-1-based movement; kinesin-1 is the principal anterograde motor for mitochondria (2–7). Elevation of $[Ca^{2+}]c$ perturbs mitochondrial transport by kinesin-1, and this effect is mediated by the outer mitochondrial membrane protein Miro1 which acts as a Ca^{2+} sensor (8,11,19). Disruption to Ca^{2+} homeostasis is seen in ALS models (29,50,51), and we show here that VAPBP56S elevates $[Ca^{2+}]c$ in transfected neurons. Moreover, we demonstrate that a Ca^{2+}-insensitive mutant of Miro1 rescues defective mitochondrial transport. The precise mechanism by which elevated $[Ca^{2+}]c$ disrupts anterograde mitochondrial transport by kinesin-1 are not properly understood, but there is evidence that it involves release of kinesin-1-bound Miro1 from tubulin (8). In line with this model, we show that VAPBP56S reduces the amount of tubulin but not kinesin-1 that is associated with Miro1 and that this effect is rescued by expression of the Ca^{2+}-insensitive mutant of Miro1. Damage to anterograde axonal transport of mitochondria by VAPBP56S may therefore involve elevation of $[Ca^{2+}]c$ which in turn induces release of Miro1 with associated kinesin-1 from microtubules to halt transport.

VAPB is an integral ER protein and VAPBP56S disrupts ER structure (26–31). The ER is a store for Ca^{2+} and recent studies have shown that VAPB functions to regulate Ca^{2+} exchange between ER and mitochondria, and that VAPBP56S is defective in this process (40). In addition, VAPB is involved in ER stress and the unfolded protein response (UPR) and there is evidence that VAPBP56S is also defective in this function although the mechanisms are controversial (29,36–39). In some reports, expression of VAPB induces UPR and VAPBP56S inhibits this process (36,37,44). In another, expression of VAPB and VAPBP56S both inhibit UPR but VAPBP56S is more potent in this effect (38). Finally, other studies have shown that VAPB and/or VAPBP56S can induce ER stress and UPR (29,39). Whatever the precise details, recent studies have shown that the UPR can influence Ca^{2+} release from ER stores (52). VAPBP56S perturbation of the ER structure and UPR may therefore impact on this process.
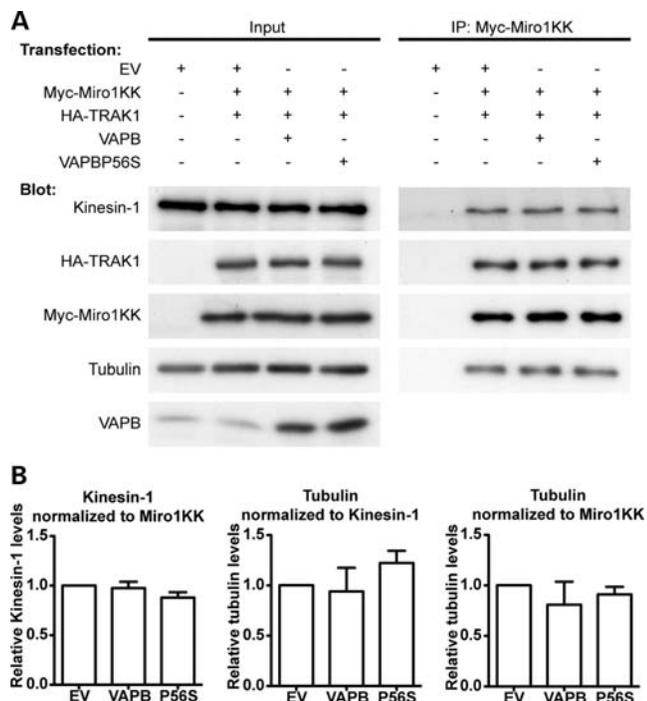
Figure 4. Expression of Ca^{2+}-insensitive Miro1$^{E208K/E328K}$ rescues the effect of VAPBP56S on the association of tubulin with Miro1. (**A**) HEK293 cells were co-transfected with either empty vector (EV), empty vector + myc-Miro1$^{E208K/E328K}$ (Myc-Miro1KK) + HA-TRAK1, VAPB + myc-Miro1$^{E208K/E328K}$ + HA-TRAK1 or VAPBP56S + myc-Miro1$^{E208K/E328K}$ + HA-TRAK1 as indicated. Miro1$^{E208K/E328K}$ was immunoprecipitated using the myc-tag and the amounts of co-immunoprecipitating kinesin-1 and α-tubulin detected by immunoblotting. Samples of the input lysates (Input) and immunoprecipitates (IP:Myc-Miro1KK) are shown. (**B**) Bar graphs show relative levels of kinesin-1 and α-tubulin in the immunoprecipitates. Kinesin-1 signals were normalized to immunoprecipitated myc-Miro1$^{E208K/E328K}$ signal; α-tubulin signals were normalized to both immunoprecipitated myc-Miro1$^{E208K/E328K}$ and immunoprecipitated kinesin-1 signals as indicated. Values were converted to so that empty vector + myc-Miro1$^{E208K/E328K}$ + HA-TRAK1 transfection was assigned a reference value of 1.0. The results shown are from three independent transfections. Statistical significance was determined by one-way ANOVA followed by Tukey's *post hoc* test. $n = 3$; error bars are SEM.

Interestingly, mutant SOD1 has also been implicated in ER stress (53), and elevated Ca^{2+} levels are also seen in the mutant SOD1 expressing cells (50). Damage to axonal transport of mitochondria seen in both VAPBP56S and mutant SOD1 familial forms of ALS may therefore be related to UPR and defective Ca^{2+} handling which in turn perturbs transport via Miro1.

MATERIALS AND METHODS

Plasmids and mutagenesis

Sequences encoding human VAPB and VAPBP56S were as described previously (31). Mammalian expression vectors for VAPB and VAPBP56S were generated by cloning of VAPB/VAPBP56S sequences into pCI-neo (Promega); amino-terminal EGFP-tagged versions were generated by cloning into pEGFP-C1. Expression vectors for myc-tagged Miro1,

HA-tagged TRAK1 and DsRed-Mito were as described previously (7,20). Glutamates 208 and 328 in the two Miro1 EF hand domains were mutated to lysine (Miro1$^{E208K/E328K}$) with oligonucleotides 5′-GGTACTCTCAATGATGCTAAACTCAACTTCTTTCAGAG-3′ and 5′-CTCTGAAAGAAGTTGAGTTTAGCATCATTGAGAGTACC-3′, and 5′-GACTGTGCTTTGTCACCTGATAAGCTTAAAGATTTATTTAAAG-3′ and 5′-CTTTAAATAAATCTTTAAGCTTATCAGGTGACAAAGCACAGTC-3′ using a QuikChange XL site-directed mutagenesis kit (Stratagene) according to the manufacturer's instructions. All constructs were verified by sequencing.

Antibodies

Mouse anti-myc tag (9B11) was from Cell Signaling Technology; rabbit anti-HA antibody was from Sigma and rabbit anti-α-tubulin was from Abcam. Antibodies to VAPB and kinesin-1 were as described previously (31,54).

Cell culture and transfection

HEK293 cells were maintained in Dulbecco's modified Eagle's medium (PAA Laboratories) containing 4.5 g/l glucose, 10% fetal bovine serum (Sera Laboratories), 2 mM L-glutamine (Invitrogen) and 1 mM sodium pyruvate (Sigma) and were transfected with ExGen500 (Fermentas) according to the manufacturer's instructions. Cells were harvested for analyses 24 h post-transfection.

Cortical neurons were isolated from embryonic day 18 rat embryos and cultured on glass cover slips coated with poly-L-lysine in 6- or 12-well plates in neurobasal medium containing B27 supplement (Invitrogen), 100 IU/ml penicillin, 100 µg/ml streptomycin and 2 mM L-glutamine. Cells were cultured for 7 days and then transfected using a calcium phosphate Profection kit (Promega) as previously described (55). For studies in HEK293 cells and neurons, all experimental treatments involved transfection of the same amounts of DNA; where several plasmids were involved, transfections were balanced by addition of control vector. For studies on the effects of Miro1 and Miro1$^{E208K/E328K}$ on axonal transport, neurons were transfected with twice the amount of Miro1 or Miro1$^{E208K/E328K}$ plasmid compared with DsRed-Mito to ensure that all cells visualized for mitochondrial transport expressed Miro1 and this was confirmed by immunostaining for the myc-tag.

Biochemical purifications

For immunoprecipitation assays, transfected cells were lysed in ice-cold immunoprecipitation buffer comprising 50 mM Tris-citrate, pH 7.4, 150 mM NaCl, 1% Triton X-100, 5 mM ethylene glycol tetraacetic acid (EGTA), 5 mM ethylenediaminetetraacetic acid and protease inhibitors (Complete, Roche) for 1 h. After centrifugation at $100\,000g$ for 40 min at 4°C, the supernatants were precleared with protein G-Sepharose beads (Sigma) for 30 min at 4°C and then incubated with primary antibody for 16 h at 4°C. Antibodies were captured with protein G-Sepharose beads and following washing with phosphate-buffered saline supplemented with 0.1% Triton X-100, bound proteins were eluted by incubation in SDS–
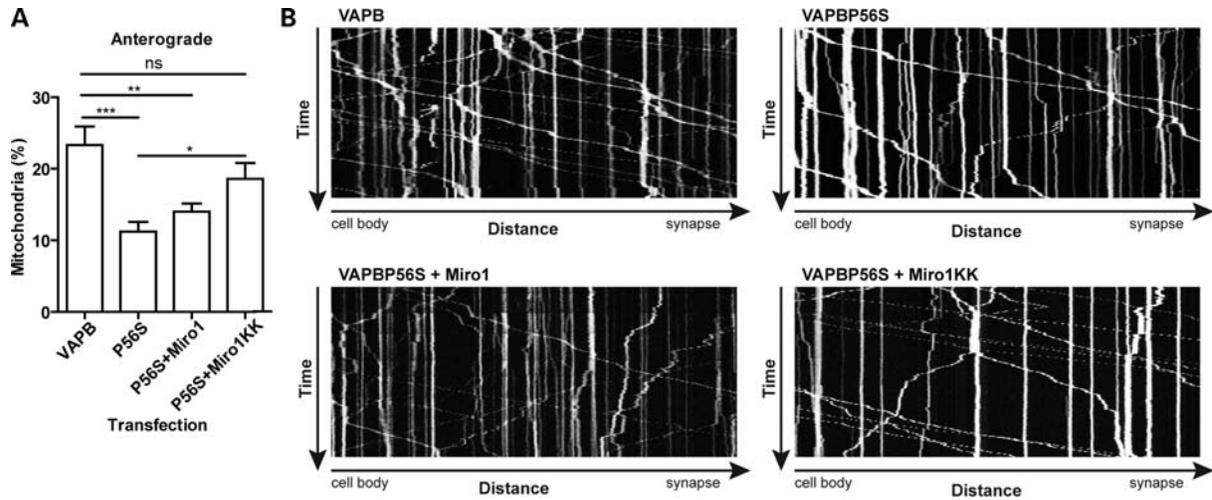
Figure 5. VAPBP56S-induced defective anterograde mitochondrial transport is rescued by expression of Ca^{2+}-insensitive $Miro1^{E208K/E328K}$. Neurons were co-transfected with DsRed-Mito and either EGFP-VAPB, EGFP-VAPBP56S, EGFP-VAPBP56S + Miro1 or EGFP-VAPBP56S + $Miro1^{E208K/E328K}$. Transfections were balanced with empty vector so that all treatments received the same total amounts of DNA. (**A**) The proportion of anterograde moving mitochondria. Expression of EGFP-VAPBP56S (P56S) reduced anterograde mitochondrial transport and this was rescued by expression of $Miro1^{E208K/E328K}$ (MiroKK) but not wild-type Miro1. Statistical significance was determined by one-way ANOVA followed by Tukey's *post hoc* test. $n = 15$–17; error bars are SEM; *$P < 0.05$, **$P < 0.01$; ***$P < 0.001$, ns not significant. (**B**) Representative kymographs of mitochondrial movement in neurons co-transfected with EGFP-VAPB (VAPB), EGFP-VAPBP56S (VAPBP56S), EGFP-VAPBP56S + Miro1 (VAPBP56S + Miro1) or EGFP-VAPBP56S + $Miro1^{E208K/E328K}$ (VAPBP56S + Miro1KK) as indicated.

PAGE sample buffer and heating at 95°C. Samples were then analysed by immunoblotting.

SDS–PAGE and immunoblotting

Samples were separated on 10% (w/v) acrylamide gels, transferred to Protran nitrocellulose membranes (Whatman) using a Transblot system (BioRad) and, following blocking with Tris–HCl buffered saline (TBS) containing 5% milk powder and 0.1% Tween-20 for 1 h at room temperature, the membranes were probed with primary antibodies in blocking buffer for 1 h at room temperature. Following washing with TBS containing 0.1% Tween-20, the blots were further probed with horseradish peroxidase-conjugated goat anti-mouse or anti-rabbit Igs and developed using an enhanced chemiluminescence system (GE Healthcare). Signals on immunoblots were quantified using ImageJ (National Institutes of Health) after scanning with an Epson Precision V700 Photo scanner essentially as described in our previous studies (43,56,57). To ensure the signals obtained were within the linear range, the mean background-corrected optical density (OD) of each signal was interpolated for an OD calibration curve created using a calibrated OD step tablet (Kodak). Only film exposures that gave OD signals within the linear range of the OD calibration curve were used for statistical analyses. For quantification of signals of kinesin-1 bound to Miro1 in the immunoprecipitation assays, signals for co-immunoprecipitating kinesin-1 were normalized to immunoprecipitated Miro1 signal. For quantification of signals of α-tubulin bound to Miro1 in the immunoprecipitation assays, signals for co-immunoprecipitating α-tubulin were normalized to both immunoprecipitated Miro1 signal and co-immunoprecipitated kinesin-1 signal.

Microscopy and image analyses

Live microscopy of mitochondrial axonal transport was performed with an Axiovert S100 microscope (Zeiss) equipped with a Lambda LS Xenon-Arc light source (Sutter Instrument Company, Novato, CA, USA), an EGFP/DsRed filterset (Chroma Technology Corp., Rockingham, VT, USA), 40× EC Plan-Neofluar 1.3 N.A. objective (Zeiss), Lambda 10-3 filter wheel (Sutter Instrument Co.) and a Photometrics Cascade-II 512B High Speed EMCCD camera (Photometrics, Tuscon, AZ, USA). 36–48 h post-transfection, neurons on cover slips were transferred to a custom observation chamber mounted on the stage of the microscope. The cells were maintained at 37°C using an objective heater (Tempcontrol 37-2, Zeiss) and 'The Box' Microscope Temperature Control System (Life Imaging Systems). Mitochondrial movements were recorded for 10 min with 3 s time-lapse interval using Metamorph software (Molecular Devices).

Image analysis was performed with ImageJ developed by Wayne Rasband (NIH, Bethesda, MD, USA; http://rsb.info.nih.gov/ij/) extended with custom plug-ins, or Metamorph. Further calculations and statistical analysis were performed using Excel (Microsoft Corporation, Redmond, WA, USA), and Prism software (GraphPad Software Inc., San Diego, CA, USA).

Calculations of mitochondrial transport parameters were as described before (20) except that overall transport of mitochondria in Figures 1 and 5 was analyzed from kymographs using the SlopeToVelocity plugin described previously (58). Briefly, this plugin calculates the velocity by measuring the distance between the position of individual mitochondria at the start and end of time-lapse recordings and dividing by the time elapsed. This yields an overall velocity of transport

that includes anterograde and retrograde movements and stationary periods. Mitochondria were subsequently classified as motile (velocity > 0.1 μm/s) or stationary (velocity ≤ 0.1 μm/s).

Calcium measurements

To measure $[Ca^{2+}]c$, neurons were loaded with 5 μM Fura2/AM (Calbiochem) in external solution (145 mM NaCl, 2 mM KCl, 5 mM NaHCO₃, 1 mM MgCl₂, 2.5 mM CaCl₂, 10 mM glucose, 10 mM HEPES pH 7.0) for 20 min at 37°C followed by washing in external solution for 20 min at 37°C. Fura2/AM sequential 340 nm and 380 nm excitation images were recorded in time-lapse mode (1 s interval) at 37°C using Meta-Fluor software (Molecular Dynamics) on an Axiovert 200M microscope (Zeiss) equipped with a Polychrome V light source (Till Photonics), Fura2 filterset (Chroma Technology Corp.), 40× 1.3NA Fluar objective (Zeiss), Lambda 10-2 filter wheel (Sutter Instrument Co.) and a Photometrics Cool-Snap HQ2 camera (Photometrics). Neurons were kept at 37°C on the microscope in a Ludin imaging chamber (Life Imaging Systems, Basel, Switzerland) using an objective heater (Temp-control 37, Zeiss) and 'The Box' Microscope Temperature Control System (Life Imaging Systems). During experiments, neurons were perfused continuously with external solution (0.5 ml/min) using an Ismatec REGLO peristaltic pump (IDEX Corporation, Glattbrugg, Switzerland). To invoke Ca^{2+} influx, 50 mM KCl was applied in external solution (NaCl was replaced with equimolar amounts of KCl) for 2 min. $[Ca^{2+}]c$ levels were calculated from the ratio of fluorescent signals at excitation 340 and 380 nm, and calibrated by sequential addition of saturating CaCl₂ (20 mM) and EGTA (20 mM) in external solution after incubation with 10 μM A23187 Ca^{2+}-ionophore (Sigma) and then translated to nanomolar using the Grynkiewicz formula (59). Resting $[Ca^{2+}]c$ was determined as the average ratio value between 60 and 180 s of recording.

ACKNOWLEDGEMENTS

We thank Pontus Aspenström (Ludwig Institute for Cancer Research, Uppsala University, Uppsala, Sweden) and Anne Stephenson (School of Pharmacy, London UK) for plasmids and Ron Vale (University of California, San Francisco, CA, USA) for the kinesin-1 antibody.

Conflict of Interest statement. None declared.

FUNDING

This work was supported by the Medical Research Council (MRC; http://www.mrc.ac.uk/index.htm) (G0501573 to C.C.J.M. and C.E.S.), the Wellcome Trust (http://www.wellcome.ac.uk/) (078662 to C.C.J.M.), the Motor Neurone Disease Association (MNDA; http://www.mndassociation.org/) (Miller6231 to C.C.J.M.) and the European Union 7th Framework Programme for RTD (http://ec.europa.eu/research/fp7) (Project MitoTarget: Grant Agreement HEALTH-F2-2008-223388 to C.C.J.M. and K.J.D.V.).

REFERENCES

1. Hollenbeck, P.J. and Saxton, W.M. (2005) The axonal transport of mitochondria. *J. Cell Sci.*, **118**, 5411–5419.
2. Glater, E.E., Megeath, L.J., Stowers, R.S. and Schwarz, T.L. (2006) Axonal transport of mitochondria requires milton to recruit kinesin heavy chain and is light chain independent. *J. Cell Biol.*, **173**, 545–557.
3. Pilling, A.D., Horiuchi, D., Lively, C.M. and Saxton, W.M. (2006) Kinesin-1 and dynein are the primary motors for fast transport of mitochondria in Drosophila motor axons. *Mol. Biol. Cell*, **17**, 2057–2068.
4. Tanaka, Y., Kanai, Y., Okada, Y., Nonaka, S., Takeda, S., Harada, A. and Hirokawa, N. (1998) Targeted disruption of mouse conventional kinesin heavy chain, kif5B, results in abnormal perinuclear clustering of mitochondria. *Cell*, **93**, 1147–1158.
5. Hurd, D.D. and Saxton, W.M. (1996) Kinesin mutations cause motor neuron disease phenotypes by disrupting fast axonal transport in Drosophila. *Genetics*, **144**, 1075–1085.
6. Cai, Q., Gerwin, C. and Sheng, Z.H. (2005) Syntabulin-mediated anterograde transport of mitochondria along neuronal processes. *J. Cell Biol.*, **170**, 959–969.
7. Fransson, S., Ruusala, A. and Aspenstrom, P. (2006) The atypical Rho GTPases Miro-1 and Miro-2 have essential roles in mitochondrial trafficking. *Biochem. Biophys. Res. Commun.*, **344**, 500–510.
8. Wang, X. and Schwarz, T.L. (2009) The mechanism of Ca^{2+}-dependent regulation of kinesin-mediated mitochondrial motility. *Cell*, **136**, 163–174.
9. Stowers, R.S., Megeath, L.J., Gorska-Andrzejak, J., Meinertzhagen, I.A. and Schwarz, T.L. (2002) Axonal transport of mitochondria to synapses depends on milton, a novel Drosophila protein. *Neuron*, **36**, 1063–1077.
10. Guo, X., Macleod, G.T., Wellington, A., Hu, F., Panchumarthi, S., Schoenfield, M., Marin, L., Charlton, M.P., Atwood, H.L. and Zinsmaier, K.E. (2005) The GTPase dMiro is required for axonal transport of mitochondria to Drosophila synapses. *Neuron*, **47**, 379–393.
11. Saotome, M., Safiulina, D., Szabadkai, G., Das, S., Fransson, A., Aspenstrom, P., Rizzuto, R. and Hajnoczky, G. (2008) Bidirectional Ca^{2+}-dependent control of mitochondrial dynamics by the Miro GTPase. *Proc. Natl Acad. Sci. USA*, **105**, 20728–20733.
12. Smith, M.J., Pozo, K., Brickley, K. and Stephenson, F.A. (2006) Mapping the GRIF-1 binding domain of the kinesin, KIF5C, substantiates a role for GRIF-1 as an adaptor protein in the anterograde trafficking of cargoes. *J. Biol. Chem.*, **281**, 27216–27228.
13. Brickley, K., Smith, M.J., Beck, M. and Stephenson, F.A. (2005) GRIF-1 and OIP106, members of a novel gene family of coiled-coil domain proteins: association *in vivo* and *in vitro* with kinesin. *J. Biol. Chem.*, **280**, 14723–14732.
14. Macaskill, A.F., Brickley, K., Stephenson, F.A. and Kittler, J.T. (2008) GTPase dependent recruitment of Grif-1 by Miro1 regulates mitochondrial trafficking in hippocampal neurons. *Mol. Cell Neurosci.*, **40**, 301–312.
15. Brickley, K. and Stephenson, F.A. (2011) Trak-mediated transport of mitochondria in axons of hippocampal neurons. *J. Biol. Chem.*, **286**, 18079–18092.
16. Yi, M., Weaver, D. and Hajnoczky, G. (2004) Control of mitochondrial motility and distribution by the calcium signal: a homeostatic circuit. *J. Cell Biol.*, **167**, 661–672.
17. Chang, D.T., Honick, A.S. and Reynolds, I.J. (2006) Mitochondrial trafficking to synapses in cultured primary cortical neurons. *J. Neurosci.*, **26**, 7035–7045.
18. Rintoul, G.L., Filiano, A.J., Brocard, J.B., Kress, G.J. and Reynolds, I.J. (2003) Glutamate decreases mitochondrial size and movement in primary forebrain neurons. *J. Neurosci.*, **23**, 7881–7888.
19. Macaskill, A.F., Rinholm, J.E., Twelvetrees, A.E., Arancibia-Carcamo, I.L., Muir, J., Fransson, A., Aspenstrom, P., Attwell, D. and Kittler, J.T. (2009) Miro1 is a calcium sensor for glutamate receptor-dependent localization of mitochondria at synapses. *Neuron*, **61**, 541–555.
20. De Vos, K.J., Chapman, A.L., Tennant, M.E., Manser, C., Tudor, E.L., Lau, K.F., Brownlees, J., Ackerley, S., Shaw, P.J., McLoughlin, D.M. *et al.* (2007) Familial amyotrophic lateral sclerosis-linked SOD1 mutants

perturb fast axonal transport to reduce axonal mitochondria content. *Hum. Mol. Genet.*, **16**, 2720–2728.

21. Bilsland, L.G., Sahai, E., Kelly, G., Golding, M., Greensmith, L. and Schiavo, G. (2010) Deficits in axonal transport precede ALS symptoms *in vivo*. *Proc. Natl Acad. Sci. USA*, **107**, 20523–20528.

22. Kasher, P.R., De Vos, K.J., Wharton, S.B., Manser, C., Bennett, E.J., Bingley, M., Wood, J.D., Milner, R., McDermott, C.J., Miller, C.C. *et al.* (2009) Direct evidence for axonal transport defects in a novel mouse model of mutant spastin-induced Hereditary Spastic Paraplegia (HSP) and human HSP patients. *J. Neurochem.*, **110**, 33–44.

23. Tarrade, A., Fassier, C., Courageot, S., Charvin, D., Vitte, J., Peris, L., Thorel, A., Mouisel, E., Fonknechten, N., Roblot, N. *et al.* (2006) A mutation of spastin is responsible for swellings and impairment of transport in a region of axon characterized by changes in microtubule composition. *Hum. Mol. Genet.*, **15**, 3544–3558.

24. Brownlees, J., Ackerley, S., Grierson, A.J., Jacobsen, N.J., Shea, K., Anderton, B.H., Leigh, P.N., Shaw, C.E. and Miller, C.C. (2002) Charcot-Marie-Tooth disease neurofilament mutations disrupt neurofilament assembly and axonal transport. *Hum. Mol. Genet.*, **11**, 2837–2844.

25. Perez-Olle, R., Lopez-Toledano, M.A., Goryunov, D., Cabrera-Poch, N., Stefanis, L., Brown, K. and Liem, R.K. (2005) Mutations in the neurofilament light gene linked to Charcot-Marie-Tooth disease cause defects in transport. *J. Neurochem.*, **93**, 861–874.

26. Nishimura, A.L., Mitne-Neto, M., Silva, H.C., Richieri-Costa, A., Middleton, S., Cascio, D., Kok, F., Oliveira, J.R., Gillingwater, T., Webb, J. *et al.* (2004) A mutation in the vesicle-trafficking protein VAPB causes late-onset spinal muscular atrophy and amyotrophic lateral sclerosis. *Am. J. Hum. Genet.*, **75**, 822–831.

27. Teuling, E., Ahmed, S., Haasdijk, E., Demmers, J., Steinmetz, M.O., Akhmanova, A., Jaarsma, D. and Hoogenraad, C.C. (2007) Motor neuron disease-associated mutant vesicle-associated membrane protein-associated protein (VAP) B recruits wild-type VAPs into endoplasmic reticulum-derived tubular aggregates. *J. Neurosci.*, **27**, 9801–9815.

28. Fasana, E., Fossati, M., Ruggiano, A., Brambillasca, S., Hoogenraad, C.C., Navone, F., Francolini, M. and Borgese, N. (2010) A VAPB mutant linked to amyotrophic lateral sclerosis generates a novel form of organized smooth endoplasmic reticulum. *FASEB J.*, **24**, 1419–1430.

29. Langou, K., Moumen, A., Pellegrino, C., Aebischer, J., Medina, I., Aebischer, P. and Raoul, C. (2010) AAV-mediated expression of wildtype and ALS-linked mutant VAPB selectively triggers death of motoneurons through a Ca-dependent ER-associated pathway. *J. Neurochem.*, **114**, 795–809.

30. Kim, S., Leal, S.S., Ben Halevy, D., Gomes, C.M. and Lev, S. (2010) Structural requirements for VAP-B oligomerization and their implication in amyotrophic lateral sclerosis-associated VAP-B(P56S) neurotoxicity. *J. Biol. Chem.*, **285**, 13839–13849.

31. Tudor, E.L., Galtrey, C.M., Perkinton, M.S., Lau, K.F., De Vos, K.J., Mitchell, J.C., Ackerley, S., Hortobagyi, T., Vamos, E., Leigh, P.N. *et al.* (2010) Amyotrophic lateral sclerosis mutant VAPB transgenic mice develop TDP-43 pathology. *Neuroscience*, **167**, 774–785.

32. Pennetta, G., Hiesinger, P., Fabian-Fine, R., Meinertzhagen, I. and Bellen, H. (2002) Drosophila VAP-33A directs bouton formation at neuromuscular junctions in a dosage-dependent manner. *Neuron*, **35**, 291–306.

33. Ratnaparkhi, A., Lawless, G.M., Schweizer, F.E., Golshani, P. and Jackson, G.R. (2008) A Drosophila model of ALS: human ALS-associated mutation in VAP33A suggests a dominant negative mechanism. *PLoS ONE*, **3**, e2334.

34. Prosser, D.C., Tran, D., Gougeon, P.Y., Verly, C. and Ngsee, J.K. (2008) FFAT rescues VAPA-mediated inhibition of ER-to-Golgi transport and VAPB-mediated ER aggregation. *J. Cell Sci.*, **121**, 3052–3061.

35. Peretti, D., Dahan, N., Shimoni, E., Hirschberg, K. and Lev, S. (2008) Coordinated lipid transfer between the endoplasmic reticulum and the Golgi complex requires the VAP proteins and is essential for Golgi-mediated transport. *Mol. Biol. Cell*, **19**, 3871–3884.

36. Kanekura, K., Nishimoto, I., Aiso, S. and Matsuoka, M. (2006) Characterization of amyotrophic lateral sclerosis-linked P56S mutation of vesicle-associated membrane protein-associated protein B (VAPB/ALS8). *J. Biol. Chem.*, **28**, 30223–30232.

37. Suzuki, H., Kanekura, K., Levine, T.P., Kohno, K., Olkkonen, V.M., Aiso, S. and Matsuoka, M. (2009) ALS-linked P56S-VAPB, an aggregated loss-of-function mutant of VAPB, predisposes motor neurons to ER stress-related death by inducing aggregation of co-expressed wild-type VAPB. *J. Neurochem.*, **108**, 973–985.

38. Gkogkas, C., Middleton, S., Kremer, A.M., Wardrope, C., Hannah, M., Gillingwater, T.H. and Skehel, P. (2008) VAPB interacts with and modulates the activity of ATF6. *Hum. Mol. Genet.*, **17**, 1517–1526.

39. Tsuda, H., Han, S.M., Yang, Y., Tong, C., Lin, Y.Q., Mohan, K., Haueter, C., Zoghbi, A., Harati, Y., Kwan, J. *et al.* (2008) The amyotrophic lateral sclerosis 8 protein VAPB is cleaved, secreted, and acts as a ligand for Eph receptors. *Cell*, **133**, 963–977.

40. De Vos, K.J., Morotz, G.M., Stoica, R., Tudor, E.L., Lau, K.F., Ackerley, S., Warley, A., Shaw, C.E. and Miller, C.C. (2012) VAPB interacts with the mitochondrial protein PTPIP51 to regulate calcium homeostasis. *Hum. Mol. Genet.* doi:10.1093/hmg/ddr559.

41. Kanekura, K., Suzuki, H., Aiso, S. and Matsuoka, M. (2009) ER Stress and unfolded protein response in amyotrophic lateral sclerosis. *Mol. Neurobiol.*, **39**, 81–89.

42. Ackerley, S., Thornhill, P., Grierson, A.J., Brownlees, J., Anderton, B.H., Leigh, P.N., Shaw, C.E. and Miller, C.C.J. (2003) Neurofilament heavy chain side-arm phosphorylation regulates axonal transport of neurofilaments. *J. Cell Biol.*, **161**, 489–495.

43. Vagnoni, A., Rodriguez, L., Manser, C., De Vos, K.J. and Miller, C.C.J. (2011) Phosphorylation of kinesin light chain-1 at serine-460 modulates binding and trafficking of calsyntenin-1. *J. Cell Sci.*, **124**, 1032–1042.

44. Chen, H.J., Anagnostou, G., Chai, A., Withers, J., Morris, A., Adhikaree, J., Pennetta, G. and de Belleroche, J.S. (2010) Characterisation of the properties of a novel mutation in VAPB in familial ALS. *J. Biol. Chem.*, **285**, 40266–40281.

45. Landers, J.E., Leclerc, A.L., Shi, L., Virkud, A., Cho, T., Maxwell, M.M., Henry, A.F., Polak, M., Glass, J.D., Kwiatkowski, T.J. *et al.* (2008) New VAPB deletion variant and exclusion of VAPB mutations in familial ALS. *Neurology*, **70**, 1179–1185.

46. Morris, R.L. and Hollenbeck, P.J. (1995) Axonal transport of mitochondria along microtubules and F-actin in living vertebrate neurons. *J. Cell Biol.*, **131**, 1315–1326.

47. Stagi, M., Gorlovoy, P., Larionov, S., Takahashi, K. and Neumann, H. (2006) Unloading kinesin transported cargoes from the tubulin track via the inflammatory c-Jun N-terminal kinase pathway. *FASEB J.*, **20**, 2573–2575.

48. Ferraiuolo, L., Kirby, J., Grierson, A.J., Sendtner, M. and Shaw, P.J. (2011) Molecular pathways of motor neuron injury in amyotrophic lateral sclerosis. *Nat. Rev. Neurol.*, **7**, 616–630.

49. De Vos, K.J., Grierson, A.J., Ackerley, S. and Miller, C.C.J. (2008) Role of axonal transport in neurodegenerative diseases. *Annu. Rev. Neurosci.*, **31**, 151–173.

50. Tradewell, M.L., Cooper, L.A., Minotti, S. and Durham, H.D. (2011) Calcium dysregulation, mitochondrial pathology and protein aggregation in a culture model of amyotrophic lateral sclerosis: mechanistic relationship and differential sensitivity to intervention. *Neurobiol. Dis.*, **42**, 265–275.

51. Grosskreutz, J., Van Den Bosch, L. and Keller, B.U. (2010) Calcium dysregulation in amyotrophic lateral sclerosis. *Cell Calcium*, **47**, 165–174.

52. Li, G., Mongillo, M., Chin, K.T., Harding, H., Ron, D., Marks, A.R. and Tabas, I. (2009) Role of ERO1-alpha-mediated stimulation of inositol 1,4,5-triphosphate receptor activity in endoplasmic reticulum stress-induced apoptosis. *J. Cell Biol.*, **186**, 783–792.

53. Saxena, S., Cabuy, E. and Caroni, P. (2009) A role for motoneuron subtype-selective ER stress in disease manifestations of FALS mice. *Nat. Neurosci.*, **12**, 627–636.

54. Niclas, J., Navone, F., Hom-Booher, N. and Vale, R.D. (1994) Cloning and localization of a conventional kinesin motor expressed exclusively in neurons. *Neuron*, **12**, 1059–1072.

55. Ackerley, S., Grierson, A.J., Brownlees, J., Thornhill, P., Anderton, B.H., Leigh, P.N., Shaw, C.E. and Miller, C.C.J. (2000) Glutamate slows axonal transport of neurofilaments in transfected neurons. *J. Cell Biol.*, **150**, 165–175.

56. Lee, J.H., Lau, K.F., Perkinton, M.S., Standen, C.L., Shemilt, S.J., Mercken, L., Cooper, J.D., McLoughlin, D.M. and Miller, C.C. (2003) The neuronal adaptor protein X11alpha reduces Abeta levels in the brains

of Alzheimer's APPswe Tg2576 transgenic mice. *J. Biol. Chem.*, **278**, 47025–47029.

57. Lee, J.H., Lau, K.F., Perkinton, M.S., Standen, C.L., Rogelj, B., Falinska, A., McLoughlin, D.M. and Miller, C.C. (2004) The neuronal adaptor protein X11beta reduces Abeta levels and amyloid plaque formation in the brains of transgenic mice. *J. Biol. Chem.*, **279**, 49099–49104.

58. De Vos, K.J. and Sheetz, M.P. (2007) Visualization and quantification of mitochondrial dynamics in living animal cells. *Methods Cell Biol.*, **80**, 627–682.

59. Grynkiewicz, G., Poenie, M. and Tsien, R.Y. (1985) A new generation of Ca^{2+} indicators with greatly improved fluorescence properties. *J. Biol. Chem.*, **260**, 3440–3450.